Research Article | Vol. 26, No. 25 | 10 Dec 2018 | OPTICS EXPRESS 32777
Optics EXPRESS

Transverse mode-switchable fiber laser based on a photonic lantern

Ning Wang,[1] J. C. Alvarado Zacarias,[1] J. Enrique Antonio-Lopez,[1] Z. Sanjabi Eznaveh,[1] Cedric Gonnet, [2] Pierre Sillard,[2] Sergio Leon-Saval,[3] Axel Schülzgen,[1] Guifang Li,[1,4] and Rodrigo Amezcua-Correa[1,5]

[1]*CREOL, The College of Optics and Photonics, University of Central Florida, Orlando, FL 32816, USA*
[2]*Prysmian Group, Parc des Industries Artois Flandres, 644 boulevard Est, Billy Berclau, 62092, Haisnes Cedex, France*
[3]*School of Physics, The University of Sydney, NSW 2006, Australia*
[4]*li@creol.ucf.edu*
[5]*r.amezcua@creol.ucf.edu*

Abstract: We propose and experimentally demonstrate an intra-cavity transverse mode-switchable fiber laser based on a mode-selective photonic lantern and a few-mode Er-doped fiber amplifier. The six lowest-order LP modes can lase independently and are switchable by changing the input port of the photonic lantern. We measured the slope efficiency, mode intensity profile, and optical spectrum of each lasing mode. In addition, we demonstrate donut-shaped LP_{11} and LP_{21} modes using incoherent superposition and simultaneous lasing of the two degenerate modes.

1. Introduction

High-order transverse mode lasers are beneficial for a number of applications. For example, high-order linear polarization (LP) modes in optical fiber have higher thresholds for detrimental nonlinear impairments, such as stimulated Brillouin scattering (SBS), compared to the fundamental mode [1]. It has also been shown that high-order modes can reduce sensitivity to mode profile distortion [2], as well as improve energy extraction in high power pulsed laser systems. There are some other important applications where the use of higher-order modes are essential; these applications range from fiber sensors [3] to the detection of gravitational waves where higher-order modes can significantly reduce the thermal noise [4,5].

Several techniques have been successfully implemented to generate lasing at specific high-order modes. For example, using a few-mode fiber Bragg grating (FBG) and a tunable filter, it is possible to select from the two lowest LP modes [6–8]. However, this method cannot yield higher-order modes due to the limited resolution of both the FBG and the filter. Similarly, employing a polarization discriminating element, lasing at the two lowest LP modes can also be achieved [9]. However, this method still cannot produce lasing at higher-order modes. A "digital laser" employing a software-defined spatial light modulator (SLM) has also been demonstrated to generate desired modes [10], but the laser efficiency is low owing to the high losses of the SLM. Another approach is dynamic intra-cavity beam control with an electronically-addressable deformable mirror [11].

Lasers with donut-shaped profiles can also be useful in many different areas. Donut beams can be used in stimulated emission depletion (STED) microscopy, in which the depletion beam has a donut-shaped profile with a dark central focal spot [12,13]. For material processing, donut beams can be used to achieve desired processed surfaces [14], as well as improve processing speed [15]. Donut-shaped lasers carrying orbital angular momentum (OAM) associate with helical phase front can be generated by tailoring the pump intensity

#343217 https://doi.org/10.1364/OE.26.032777
Journal © 2018 Received 31 Aug 2018; revised 14 Nov 2018; accepted 14 Nov 2018; published 29 Nov 2018

Optics EXPRESS

distribution [16,17] or by placing a set of phase plates inside a folded cavity [18]. Recently, an intra-cavity donut mode laser was reported that was generated by an incoherent superposition of two degenerate petal modes lasing together in the same cavity [19]. Donut-shaped profile lasers could also be generated in an all-fiber laser structure by using mode-selective elements such as few-mode FBGs [7] or mode-selective couplers [20].

In this work, we demonstrate a transverse mode-switchable erbium-doped fiber laser based on a 6-mode-selective photonic lantern (MSPL). Our preliminary results were reported in [21]. The output mode of the laser can be easily switched among the six lowest-order LP modes by simply changing the input port of the photonic lantern (PL). Their slope efficiencies, mode intensity profiles, optical spectra, and optical signal-to-noise ratios (OSNR) were characterized. Using the same configuration, we also generated donut-shaped LP_{11} and LP_{21} modes using incoherent superposition and simultaneous lasing of the two degenerate modes. Their circular shaped intensity profiles were clearly observed. To the best of our knowledge, this work reports the largest number of intra-cavity transverse modes that has been achieved in an all-fiber laser structure.

2. Principle and experimental setup

In general, MSPLs are passive all-fiber devices capable of efficiently multiplexing single-mode inputs and converting each input into a specific LP mode. Among other applications, the PL has great potential for space-division multiplexing (SDM) [22–24], as well as spatial mode control for high power fiber amplifiers [25]. In general, a PL consist of a set of single mode fibers (SMFs) inserted into a capillary tube whose index of refraction is lower than the refractive index of the SMF cladding. The tube is adiabatically tapered down to create an few-mode fiber (FMF) output at the taper waist [26,27], as shown in Fig. 1(a). The mode selectivity feature can be obtained if the input SMF core sizes are different. Each input fundamental mode evolves into a particular mode in the output FMF that has a matching propagation constant [28,29]. Figure 1(b) shows a schematic input cross sectional profile of a 6-mode MSPL [30]. It contains 6 graded-index fibers with core diameters of 23, 18, 18, 15, 15, and 11μm, which map to the LP_{01}, LP_{11a}, LP_{11b}, LP_{21a}, LP_{21b}, and LP_{02} mode, respectively. After tapering, the resulting FMF's cladding diameter is 110 μm while the core diameter is 20 μm. The refractive index contrast of the core and the fluorine-doped silica capillary is $\Delta n = 9.5 \times 10^{-3}$. The output facet of the PL can be easily spliced with a 6-mode FMF, which has a core and cladding diameter of 16/125 μm. The mode profiles at the output of the spliced FMF were measured at 1550 nm and are shown in Fig. 1(c). We can clearly see that the six lowest order LP modes are well preserved after they propagate through the FMF.

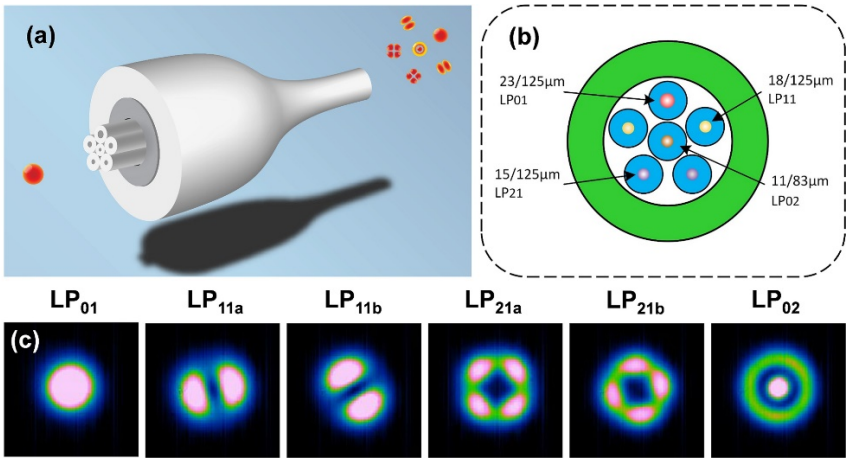

Fig. 1. (a) Schematic of a MSPL; (b) cross-sectional view of the input fiber distribution in the MSPL; (c) mode profiles of the PL after splicing to a 6-mode FMF at λ = 1550 nm.

Optics EXPRESS

The fabricated MSPL has mode-dependent losses (MDL) as a consequence of imperfections in the PL taper. The total losses of the PL (including insertion loss and splice loss) for both pump and signal wavelength were measured, the results are shown in Table 1. We found the loss for the LP_{02} mode was larger than for other LP modes at both wavelengths.

Table 1. Losses of the MSPL at both pump and signal wavelength (in dB)

	LP_{01}	LP_{11a}	LP_{11b}	LP_{21a}	LP_{21b}	LP_{02}
976 nm	0.88	1.66	0.55	0.98	0.96	2.97
1550 nm	1.71	3.75	1.79	2.29	1.46	4.35

The gain media used in this experiment was an erbium-doped few-mode fiber (ED-FMF) which was fabricated in house [31]. Figure 2(a) shows the measured refractive index profile of this fiber, and Fig. 2(b) shows a microscope image of the ED-FMF cross section. The core and cladding diameters of the ED-FMF are 13 μm and 163 μm, respectively, with a step-index profile. The estimated numerical aperture (NA) was 0.249, ensuring that more than 6 LP modes were supported at λ = 1550 nm. The core area was uniformly doped with pure erbium ions at a dopant density of 4.5×10^{25} m^{-3}, which supports a maximum gain of nearly 10 dB/m for each spatial mode at 1550 nm [32]. We spliced the ED-FMF with the passive 6-mode FMF and measured the mode profile of each LP mode at the output, the results are shown in Fig. 2(c). We can see that the higher-order modes (LP_{21} and LP_{02}) are slightly distorted due to the core size mismatch.

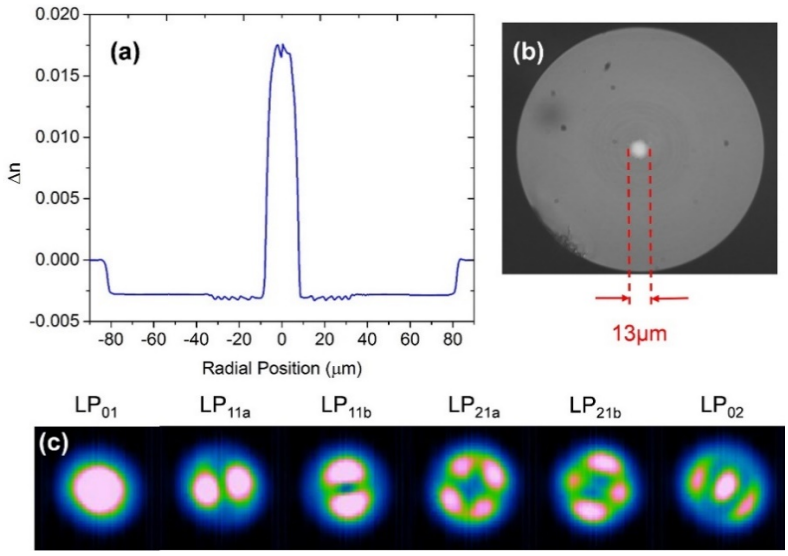

Fig. 2. (a) Measured refractive index of the ED-FMF; (b) cross-sectional image of the ED-FMF; (c) mode profiles from ED-FMF spliced with 6-mode FMF.

Figure 3 shows the experimental setup of the mode-switchable fiber laser. Light from the pump diode (pigtail fiber type: SM98-PS-U25A) with a central wavelength of 976 nm travels through a polarization controller (PC) to optimize the injected power. After the PC was a wavelength-division multiplexer (WDM) (fiber type: HI1060 FLEX). The other input port of the WDM was connected to a fiber Bragg grating (FBG) with a central wavelength of 1536.8 nm and a reflection bandwidth of 0.6 nm. The FBG was made of standard SMF, the reflectivity of the FBG was measured as 60%. In order to generate the desired laser mode, the output of the WDM could be switched to any one of the six input SMFs of the PL. On the other side, the output of the PL was first spliced to a 1 m passive 6-mode FMF, which was then spliced to a 5 m long ED-FMF. The intermeadiate passive FMF reduced the splicing loss

that would occur between the PL and gain fiber due to the mismatch in their core sizes. The end of the ED-FMF was cleaved to be flat, yielding a 4% Fresnel reflection coefficient. The laser cavity was formed between the FBG and the end of EDF. Within each round trip, only one specific LP mode can pass through the lantern and be amplified. Hence, it should be noted that our pump and signal are the same mode which is beneficial for maximizing the amplifier gain. The laser output was focused using a 20X objective lens, and a band-pass filter at 1540 nm with a full-width half-maximum bandwidth of 12 nm was placed right after the lens to block the residual pump light. We measured the laser output power using a power meter, and the laser mode profiles using a CCD camera, as illustrated in Fig. 3.

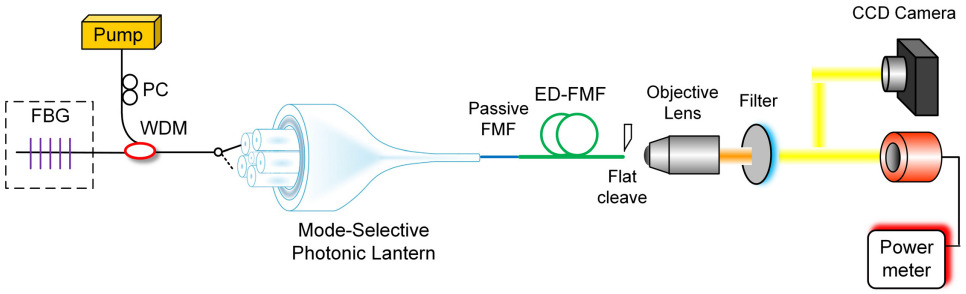

Fig. 3. Experimental setup for the transverse mode-switchable fiber laser. The MSPL is used to switch between different LP modes. PC: polarization controller; FBG: fiber Bragg grating.

3. Results and discussions

3.1 LP modes laser results

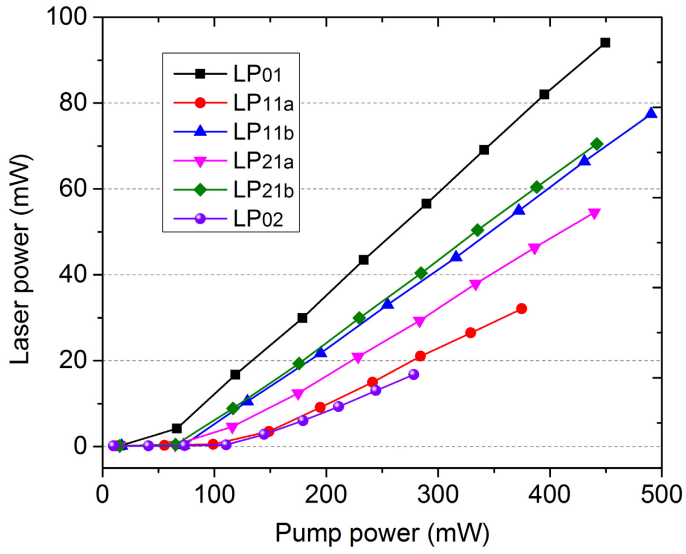

Fig. 4. Output power vs. pump power for the six lasing modes.

The measured output laser powers versus pump power for all 6 lasing modes are shown in Fig. 4. The horizontal axis shows the pump power measured at the passive FMF output. It should be noted that there are splicing losses between the passive FMF and the gain fiber, and the losses are different for each LP mode, so the absorbed pump powers are smaller than the values shown in Fig. 4 and are not the same for all the pump modes. From Fig. 4, we can see that all six LP modes can lase when the pump power surpasses their threshold. The LP_{01} lasing mode has the highest output power at >90 mW, with a slope efficiency of 23.6%. The

Optics EXPRESS

slope efficiencies for LP_{11a}, LP_{11b}, LP_{21a}, LP_{21b} and LP_{02} lasing modes are 12.8%, 18.7%, 16%, 19.2%, and 10.9%, respectively. The difference in slope efficiencies and threshold values are mainly due to the MDL of the PL at the signal wavelength and different overlap integrals between the pump and signal mode intensity profiles. The overlap integral can be expressed as [33,34]:

$$\eta_{i,j} = \iint \Gamma_{s,i}(r,\varphi)\Gamma_{p,j}(r,\varphi)N_0(r,\varphi)rdrd\varphi \quad (1)$$

where $\Gamma_{s,i}(r,\varphi)$ and $\Gamma_{p,j}(r,\varphi)$ are the normalized intensity distribution of i-th signal mode and j-th pump mode inside the ED-FMF and $N_0(r,\varphi)$ is the doping profile of the gain fiber, which is uniformly doped for our ED-FMF. In order to increase the slope efficiency, a FBG with higher reflectivity or a lower-loss MSPL, to reduce round trip loss, can be used. To decrease the threshold pump power, the EDF output can be angle cleaved and an output coupler with high reflectivity can be added to the end of the gain fiber to further reduce cavity loss.

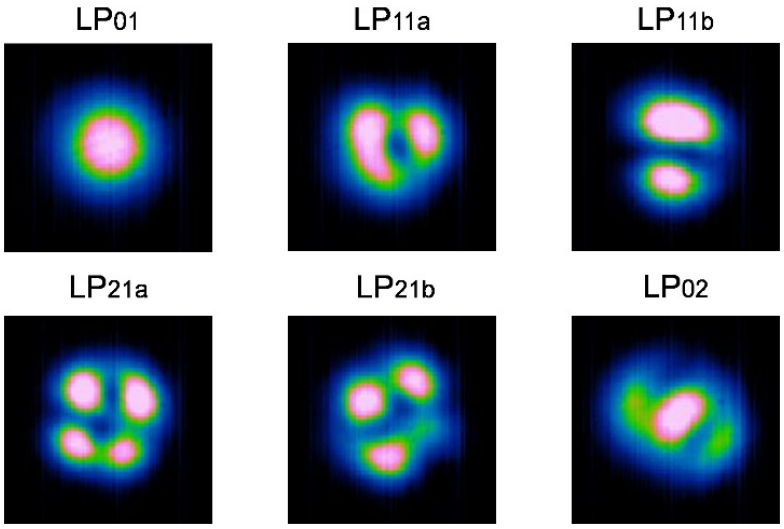

Fig. 5. Intensity profiles of the six lasing LP modes.

Regrading to the obtained mode profiles, we fixed the laser power of each lasing mode to be 15 mW, and used a CCD camera (Xenics Xeva-1.7-320) to capture their mode intensity profiles. Two attenuators were used in front of the CCD camera to prevent saturation. The camera images of the mode intensity profiles are shown in Fig. 5. It is important to highlight that all six laser mode patterns do not suffer greater distortions during the lasing operation, compare to Fig. 2(c). For the five lowest-order (LP_{01}, LP_{11s} and LP_{21s}) lasing modes, their profiles are almost ideal, but slightly distorted. This was likely due to mode crosstalk of the PL, leading to some of the single-mode input ports exciting multiple modes in the ED-FMF. Another reason could be residual mode coupling within the ED-FMF. For the LP_{02} mode, its mode profile does not look as well. This is mainly due to the core size mismatch at the splice between the passive FMF and ED-FMF. The mode profile will be distorted after propagating in the ED-FMF, as shown in Fig. 2(c). When propagated through the gain fiber, the mode profile will degrade compared to the result from the passive FMF. This problem can be fixed by using an ED-FMF whose core size better matches the 6-mode FMF core size. The mode profiles of the six LP modes didn't change as laser power increased, and were stable at room temperature. It is worth mentioning that even higher-order lasing modes could be generated if the 6-mode MSPL was replaced by a 10-mode or 15-mode MSPL [35,36].

Optics EXPRESS

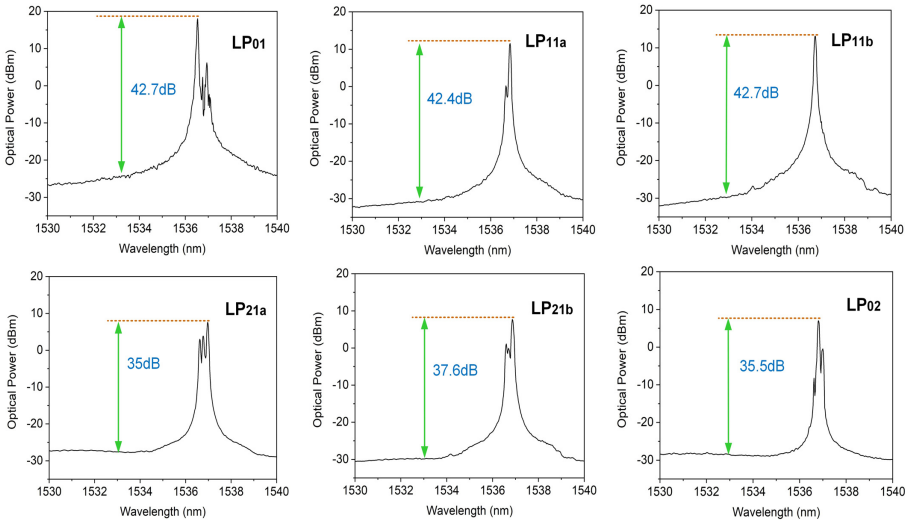

Fig. 6. Output optical spectra of the six lasing modes measured by an optical spectrum analyzer with a resolution of 0.1 nm.

In the following, we measured the optical spectra of the output lasing modes using an optical spectrum analyzer (OSA) with a 50/125 μm graded-index optical fiber input port (Ando AQ-6315e), capable of accepting high-order modes. By inserting the end of ED-FMF into a bare fiber adapter and further connecting to the input port of the OSA, we could observe the optical spectrum of each mode, as shown in Fig. 6. The resolution of the OSA was set to be 0.1 nm. The pump power was fixed at 484 mW. From Fig. 6, we find that all six modes have a central wavelength near 1537 nm and a bandwidth less than 1 nm. This matches well with the reflection spectrum of the FBG. It also indicates that the OSNR for all six lasing modes was above 35 dB, ranging from 35 dB to 42.7 dB. Note for some modes, multiple longitudinal modes are observed. There are several sidebands apart from the main peak. These sidebands are believed to be caused by the mode crosstalk of the MSPL. When the gain is high enough, the modes produced by crosstalk of the MSPL can also lase. Since different LP modes have different effective indices in the ED-FMF, they may lase at slightly different wavelengths within the reflection bandwidth of FBG, with a lower peak power compared to the selected LP mode.

3.2 Donut-shaped modes laser results

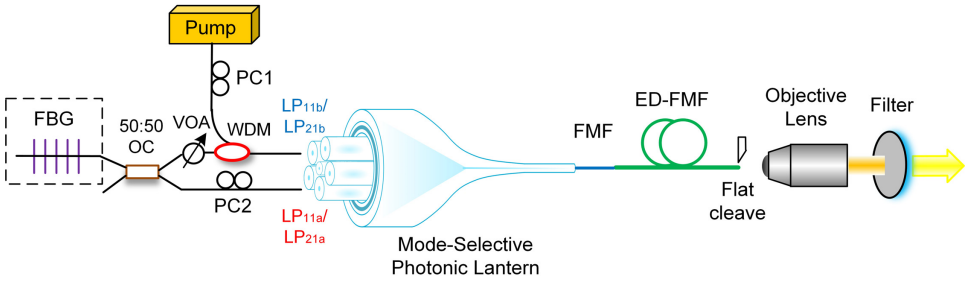

Fig. 7. Schematic of a fiber laser for the generation of donut-shaped modes by the incoherent superposition of degenerate LP_{11s} or LP_{21s} modes. OC: optical coupler; VOA: variable optical attenuator.

Next, we focus on obtaining a donut-shaped mode profile. Laser emission with a donut-shaped mode profile was generated by the incoherent superposition of two degenerate LP

Optics EXPRESS

modes. The experimental setup used to obtain this type of beam is shown in Fig. 7, only the SMF side was modified compared to the setup for generating LP modes. When the light was reflected back from the FBG, it was split into two arms by a 3dB optical coupler (OC). The upper arm went through a variable optical attenuator (VOA) that then connected to the signal port of the WDM. The output of WDM was then connected to either the LP_{11b} or LP_{21b} input port of the PL, and the lower arm of the OC was connected to the corresponding LP_{11a} or LP_{21a} port of the PL. When the upper channel is pumped, both channels can lase together with the same gain media. Since the two lasing modes go through different cavities, the output laser could be an incoherent superposition of the two degenerate modes. We adjusted PC2 to ensure the orientation of the two degenerate modes are orthogonal with respect to each other. Thus the superposition of the two degenerate LP modes is a donut-shaped mode. Both donut LP_{11} and LP_{21} modes were generated using our setup. It should be noticed that a VOA was employed to adjust the laser power between the two lasing modes. Otherwise, the laser power of the two modes could be different and would cause the output mode profile to be non-circularly symmetric. Using the same band pass filter to block the pump light, we measured both the laser power and the mode intensity profiles.

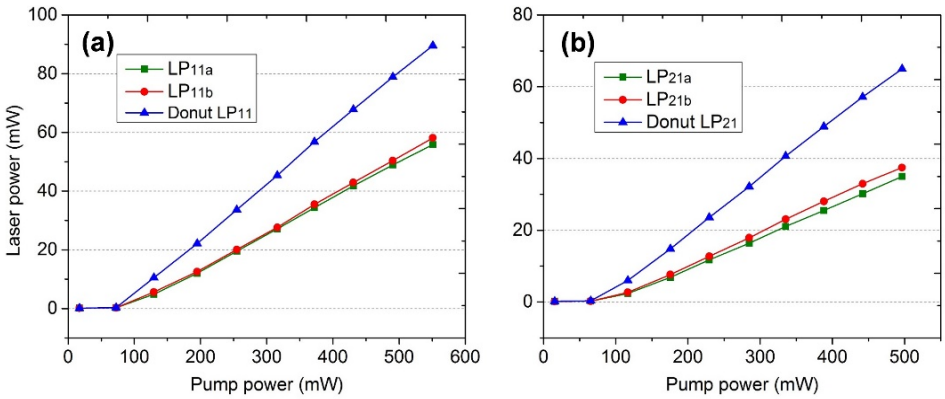

Fig. 8. Laser power vs pump power for each LP mode lasing separately and the donut mode as their incoherent superposition for the (a) LP_{11} modes and (b) LP_{21} modes.

First, we measured the laser power of each degenerate LP mode separately. We disconnected the signal port of the WDM coupler to measure the laser power of LP_{11a} mode, then, we disconnected the LP_{11a} port of the PL to measure the laser power of LP_{11b} mode. We performed these measurements by gradually increasing the attenuation of the VOA to make sure the laser power of the two modes were almost the same. Finally, both channels were connected to measure the result of the donut LP_{11} mode. The same measurements were performed for the LP_{21} modes. The results are shown in Fig. 8. The slope efficiency for the two degenerate LP_{11} modes were 12.4% and 12.8% and the result of the donut LP_{11} mode was 18.9%. The laser output power of the donut-shaped mode was 89.5 mW at a pump power of 551 mW. The slope efficiency of single LP_{21a} and LP_{21b} laser modes were 8.8% and 9.4% and the slope for the donut LP_{21} mode was 15.7%. The laser output power of the donut LP_{21} mode was measured to be 65 mW when the pump power was 496 mW.

Compared to Fig. 4, we find that at the same pump power, the laser power of each LP mode lasing individually is smaller than the result in Fig. 4. This is due to the 3dB coupler in the laser cavity, that for each round trip causes 6 dB of additional loss, which negatively contributes to the laser power. According to Fig. 8, the laser power of the donut mode is always smaller than the sum of two degenerate LP modes due to gain saturation.

Optics EXPRESS

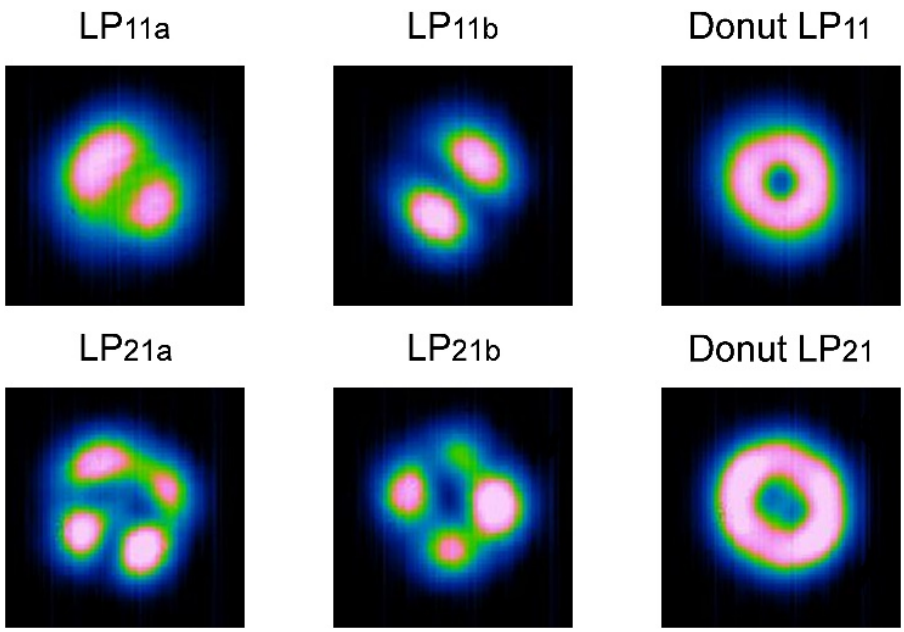

Fig. 9. Upper row: mode profiles for each LP_{11} mode lasing individually and the donut LP_{11} mode from their incoherent superposition; lower row: mode profiles for each LP_{21} mode and the donut-shaped LP_{21} mode.

Coming back to the obtained mode profiles for the donut-shaped laser scheme, the results are shown in Fig. 9. The upper row shows the mode profiles of each LP_{11} mode lasing individually and their incoherent superposition, which is the donut LP_{11} mode. The lower row shows the results for each LP_{21} modes lasing separately, as well as the donut LP_{21} mode. The results of the four degenerate LP_{11s} and LP_{21s} mode are similar to the single LP laser mode results shown in Fig. 5. And when two degenerate LP modes lase together, the donut shaped laser mode profiles are clearly observed. Both donut LP_{11} and LP_{21} modes have a circular mode intensity profile, as shown in Fig. 9. However, the donut modes are not perfectly symmetric. This is due to imperfections in the mode profiles of each degenerate LP mode.

To verify the incoherence of the donut mode laser, we conducted an interference experiment. Its working principle was described in [19]. The donut LP_{11} mode was selected for demonstration purposes because it can be easily observed due to its larger pedal size. Figure 10(a) shows a schematic of the setup for the interference experiment. We let the donut beam passed through a double pinhole, and the resultant interference pattern was viewed on a screen. The shape of the pinholes was square. The position of the pinholes corresponded to the lobes of the donut mode laser as depicted in Fig. 10(b). When points 1 and 2 are interfered, because they come from the same LP_{11} mode, strong fringes should be observed. However, when points 1 and 3 are interfered, because they are generated by two incoherent source, we should see no interference fringes.

The interference result of points 1 and 2 is shown in Fig. 10(c). Strong fringes can clearly be seen, as was expected. Conversely, no fringes can be seen when interfering points 1 and 3, as shown in Fig. 10(d). The fringes on the edge of the pattern in Fig. 10(d) are the diffraction pattern from the square shaped pinhole, which is a sinc function in two-dimensional, not from interference between two beams.

Optics EXPRESS

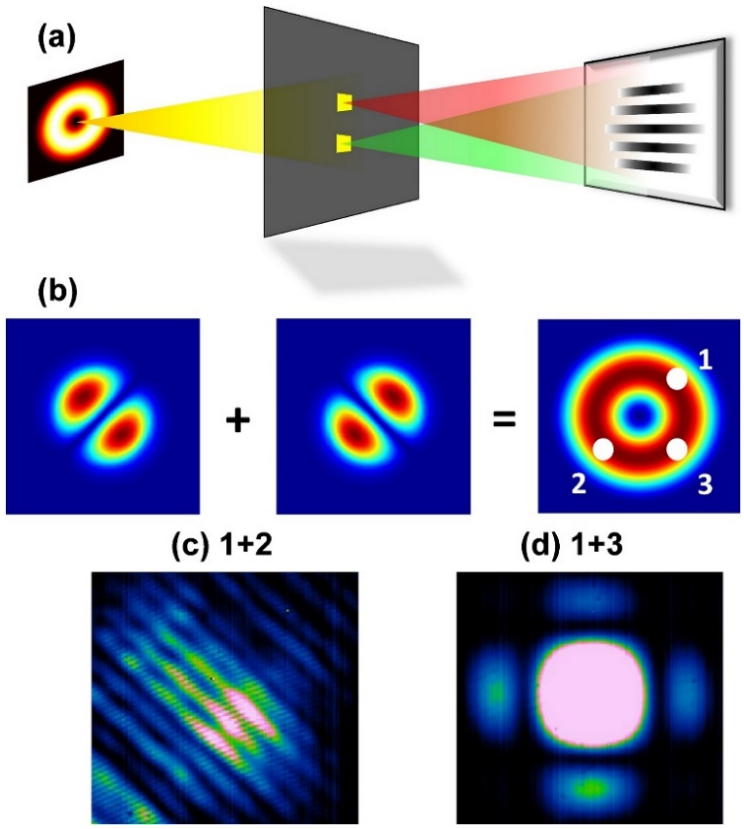

Fig. 10. (a) Schematic setup of interference experiment to verify the incoherence of the donut mode laser; (b) position of the pinholes correspond to the lobes on the donut mode laser; and the interference patterns between points 1 and 2 (c) and points 1 and 3 (d).

4. Conclusion

We have successfully demonstrated a transverse mode-switchable fiber laser using a 6-mode MSPL. The selection among different LP modes was realized by switching the input port of the PL. The slope efficiencies of the 6 lasing modes ranged from 23.6% to 10.9%, and their OSNRs ranged from 35 dB to 42.7 dB. Their mode profiles were observed using a CCD camera. All six LP modes can be clearly recognized. With the incoherent combination of degenerate LP_{11s} or LP_{21s} modes, donut shaped modes were obtained. The laser efficiencies of the donut LP_{11} and LP_{21} mode were 18.9% and 15.7%, respectively. Their circular shaped mode profiles were clearly observed. A double pinhole interference experiment was deployed to verify the incoherent superposition of our donut modes.

Funding

Army Research Office (ARO) (W911NF-17-1-0553, W911NF-17-1-0500, W911NF-12-1-0450); National Science Foundation (NSF) (ECCS-1711230).

Acknowledgments

The authors would like to thank Rachel Sampson for assistance in editing the manuscript.

Disclosures

The authors declare that there are no conflicts of interest related to this article.

Optics EXPRESS

References

1. S. Ramachandran, J. M. Fini, M. Mermelstein, J. W. Nicholson, S. Ghalmi, and M. F. Yan, "Ultra-large effective area higher order mode fibers: a new strategy for high power laser," Laser Photonics Rev. **2**(6), 429–448 (2008).
2. J. M. Fini and S. Ramachandran, "Natural bend-distortion immunity of higher-order-mode large-mode-area fibers," Opt. Lett. **32**(7), 748–750 (2007).
3. A. V. Newkirk, J. E. Antonio-Lopez, A. Velazquez-Benitez, J. Albert, R. Amezcua-Correa, and A. Schülzgen, "Bending sensor combining multicore fiber with a mode-selective photonic lantern," Opt. Lett. **40**(22), 5188–5191 (2015).
4. S. Chelkowski, S. Hild, and A. Freise, "Prospects of higher-order Laguerre-Gauss modes in future gravitational wave detectors," Phys. Rev. D Part. Fields Gravit. Cosmol. **79**(12), 122002 (2009).
5. A. Noack, C. Bogan, and B. Willke, "Higher-order Laguerre-Gauss modes in (non-) planar four-mirror cavities for future gravitational wave detectors," Opt. Lett. **42**(4), 751–754 (2017).
6. J. M. O. Daniel and W. A. Clarkson, "Rapid, electronically controllable transverse mode selection in a multimode fiber laser," Opt. Express **21**(24), 29442–29448 (2013).
7. B. Sun, A. Wang, L. Xu, C. Gu, Y. Zhou, Z. Lin, H. Ming, and Q. Zhan, "Transverse mode switchable fiber laser through wavelength tuning," Opt. Lett. **38**(5), 667–669 (2013).
8. L. Li, M. Wang, T. Liu, J. Leng, P. Zhou, and J. Chen, "High-power, cladding-pumped all-fiber laser with selective transverse mode generation property," Appl. Opt. **56**(17), 4967–4970 (2017).
9. D. Lin and W. A. Clarkson, "Polarization-dependent transverse mode selection in an Yb-doped fiber laser," Opt. Lett. **40**(4), 498–501 (2015).
10. S. Ngcobo, I. Litvin, L. Burger, and A. Forbes, "A digital laser for on-demand laser modes," Nat. Commun. **4**(1), 2289 (2013), doi:10.1038/ncomms3289.
11. W. Lubeigt, G. Valentine, J. Girkin, E. Bente, and D. Burns, "Active transverse mode control and optimization of an all-solid-state laser using an intracavity adaptive-optic mirror," Opt. Express **10**(13), 550–555 (2002).
12. B. Harke, J. Keller, C. K. Ullal, V. Westphal, A. Schönle, and S. W. Hell, "Resolution scaling in STED microscopy," Opt. Express **16**(6), 4154–4162 (2008).
13. D. Wildanger, J. Bückers, V. Westphal, S. W. Hell, and L. Kastrup, "A STED microscope aligned by design," Opt. Express **17**(18), 16100–16110 (2009).
14. J. Hamazaki, R. Morita, K. Chujo, Y. Kobayashi, S. Tanda, and T. Omatsu, "Optical-vortex laser ablation," Opt. Express **18**(3), 2144–2151 (2010).
15. M. Meier, V. Romano, and T. Feurer, "Material processing with pulsed radially and azimuthally polarized laser radiation," Appl. Phys., A Mater. Sci. Process. **86**(3), 329–334 (2007).
16. D. Lin, J. M. O. Daniel, and W. A. Clarkson, "Controlling the handedness of directly excited Laguerre-Gaussian modes in a solid-state laser," Opt. Lett. **39**(13), 3903–3906 (2014).
17. D. J. Kim and J. W. Kim, "Direct generation of an optical vortex beam in a single-frequency Nd:YVO4 laser," Opt. Lett. **40**(3), 399–402 (2015).
18. D. Naidoo, F. S. Roux, A. Dudley, I. Litvin, B. Piccirillo, L. Marrucci, and A. Forbes, "Controlled generation of higher-order Poincaré sphere beams from a laser," Nat. Photonics **10**(5), 327–332 (2016).
19. I. A. Litvin, S. Ngcobo, D. Naidoo, K. Ait-Ameur, and A. Forbes, "Doughnut laser beam as an incoherent superposition of two petal beams," Opt. Lett. **39**(3), 704–707 (2014).
20. T. Wang, F. Shi, Y. Huang, J. Wen, Z. Luo, F. Pang, T. Wang, and X. Zeng, "High-order mode direct oscillation of few-mode fiber laser for high-quality cylindrical vector beams," Opt. Express **26**(9), 11850–11858 (2018).
21. N. Wang, J. E. Antonio-Lopez, J. A. Zacarias, Z. S. Eznaveh, H. Wen, P. Sillard, S. Leon-Saval, A. Schulzgen, R. Amezcua-Correa, and G. Li, "Mode-Selective Fiber Laser Using a Photonic Lantern," in *ECOC 2016; 42nd European Conference on Optical Communication; Proceedings of*, (VDE, 2016), paper Tu2F.5.
22. H. Liu, H. Wen, J. C. A. Zacarias, J. E. Antonio-Lopez, N. Wang, P. Sillard, A. Amezcua-Correa, R. Amezcua-Correa, and G. Li, "3×10 Gb/s mode group-multiplexed transmission over a 20 km few-mode fiber using photonic lanterns," in *Optical Fiber Communication Conference*, (Optical Society of America, 2017), paper M2D.5.
23. J. Van Weerdenburg, R. Ryf, J. C. Alvarado-Zacarias, R. A. Alvarez-Aguirre, N. K. Fontaine, H. Chen, R. Amezcua-Correa, T. Koonen, and C. Okonkwo, "138 Tbit/s transmission over 650 km graded-index 6-mode fiber," in *Optical Communication (ECOC), 2017 European Conference on*, (IEEE, 2017), paper Th.PDP.A.4.
24. S. G. Leon-Saval, N. K. Fontaine, and R. Amezcua-Correa, "Photonic lantern as mode multiplexer for multimode optical communications," Opt. Fiber Technol. **35**, 46–55 (2017).
25. S. Wittek, R. Bustos Ramirez, J. Alvarado Zacarias, Z. Sanjabi Eznaveh, J. Bradford, G. Lopez Galmiche, D. Zhang, W. Zhu, J. Antonio-Lopez, L. Shah, and R. Amezcua Correa, "Mode-selective amplification in a large mode area Yb-doped fiber using a photonic lantern," Opt. Lett. **41**(10), 2157–2160 (2016).
26. N. K. Fontaine, R. Ryf, J. Bland-Hawthorn, and S. G. Leon-Saval, "Geometric requirements for photonic lanterns in space division multiplexing," Opt. Express **20**(24), 27123–27132 (2012).
27. B. Huang, N. K. Fontaine, R. Ryf, B. Guan, S. G. Leon-Saval, R. Shubochkin, Y. Sun, R. Lingle, Jr., and G. Li, "All-fiber mode-group-selective photonic lantern using graded-index multimode fibers," Opt. Express **23**(1), 224–234 (2015).
28. S. G. Leon-Saval, N. K. Fontaine, J. R. Salazar-Gil, B. Ercan, R. Ryf, and J. Bland-Hawthorn, "Mode-selective photonic lanterns for space-division multiplexing," Opt. Express **22**(1), 1036–1044 (2014).

Optics EXPRESS

29. S. Yerolatsitis, I. Gris-Sánchez, and T. A. Birks, "Adiabatically-tapered fiber mode multiplexers," Opt. Express **22**(1), 608–617 (2014).
30. A. M. Velazquez-Benitez, J. C. Alvarado, G. Lopez-Galmiche, J. E. Antonio-Lopez, J. Hernández-Cordero, J. Sanchez-Mondragon, P. Sillard, C. M. Okonkwo, and R. Amezcua-Correa, "Six mode selective fiber optic spatial multiplexer," Opt. Lett. **40**(8), 1663–1666 (2015).
31. G. Lopez-Galmiche, Z. Sanjabi Eznaveh, J. E. Antonio-Lopez, A. M. Velazquez Benitez, J. Rodriguez Asomoza, J. J. Sanchez Mondragon, C. Gonnet, P. Sillard, G. Li, A. Schülzgen, C. M. Okonkwo, and R. Amezcua Correa, "Few-mode erbium-doped fiber amplifier with photonic lantern for pump spatial mode control," Opt. Lett. **41**(11), 2588–2591 (2016).
32. N. K. Fontaine, B. Huang, Z. S. Eznaveh, H. Chen, J. Cang, B. Ercan, A. Veláquez-Benitez, S. H. Chang, R. Ryf, A. Schulzgen, J. C. A. Zaharias, P. Sillard, C. Gonnet, J. E. A. Lopez, and R. Amezcua-Correa, "Multi-mode optical fiber amplifier supporting over 10 spatial modes," in *Optical Fiber Communication Conference*, (Optical Society of America, 2016), paper Th5A.4.
33. N. Bai, E. Ip, T. Wang, and G. Li, "Multimode fiber amplifier with tunable modal gain using a reconfigurable multimode pump," Opt. Express **19**(17), 16601–16611 (2011).
34. E. Ip, "Gain equalization for few-mode fiber amplifiers beyond two propagating mode groups," IEEE Photonics Technol. Lett. **24**(21), 1933–1936 (2012).
35. A. Velázquez-Benítez, J. Antonio-López, J. Alvarado-Zacarías, G. Lopez-Galmiche, P. Sillard, D. Van Ras, C. Okonkwo, H. Chen, R. Ryf, N. Fontaine, and R. Amezcua-Correa, "Scaling the fabrication of higher order photonic lanterns using microstructured preforms," in *Optical Communication (ECOC), 2015 European Conference on*, (IEEE, 2015), paper Tu.3.3.2.
36. A. M. Velázquez-Benítez, J. E. Antonio-López, J. C. Alvarado-Zacarías, N. K. Fontaine, R. Ryf, H. Chen, J. Hernández-Cordero, P. Sillard, C. Okonkwo, S. G. Leon-Saval, and R. Amezcua-Correa, "Scaling photonic lanterns for space-division multiplexing," Sci. Rep. **8**(1), 8897 (2018).